Structural and rheological changes of lamellar liquid crystals as a result of compositional changes and added silica nanoparticles

Journal:	*Physical Chemistry Chemical Physics*
Manuscript ID	CP-ART-04-2018-002101.R1
Article Type:	Paper
Date Submitted by the Author:	24-May-2018
Complete List of Authors:	Marlow, Joshua; Monash University, Pottage, Matthew; Monash University, School of Chemistry McCoy, Thomas; Monash University, School of Chemistry de Campo, Liliana; ANSTO, ACNS Sokolova, Anna; ANSTO, ACNS Bell, Toby; Monash University, School of Chemistry Tabor, Rico; Monash University, School of Chemistry

Journal Name

ARTICLE TYPE

Cite this: DOI: 10.1039/xxxxxxxxxx

Structural and rheological changes of lamellar liquid crystals as a result of compositional changes and added silica nanoparticles

Joshua B. Marlow,[a] Matthew J. Pottage[a], Thomas M. McCoy[a], Liliana De Campo[b], Anna Sokolova[b], Toby D.M. Bell,[a] and Rico F. Tabor*[a]

Received Date
Accepted Date

DOI: 10.1039/xxxxxxxxxx

www.rsc.org/journalname

Lamellar liquid crystals comprising oil, water and surfactant(s) were formulated and analysed in order to examine how these materials responded to the inclusion of inorganic nanoparticles, in terms of their structural and rheological characteristics. Lamellar phases were formed from mixtures of water, *para*-xylene and Triton X-100, and analysis was performed via small-angle neutron scattering (SANS), polarising light microscopy (PLM), and amplitude and viscosity sweeps. The partial replacement of Triton X-100 with oleic acid appeared to cause an increase in bilayer thickness, attributed to less efficient packing of the different molecules. Addition of oleic acid also appeared to cause both a loss in lamellar repeat ordering, attributed to heterogeneity of the bilayers, and a rise in long range order, potentially caused by the stiffer bilayers. Adding silica nanoparticles of different size and surface chemistry caused a stiffening of the samples at the expense of a longer-range lamellar repeat order. This strengthening is attributed to aggregation at the domain boundaries, and it was found that hydrophobic particles tended to form stronger aggregates while for larger particles (20 nm as opposed to 10 nm) aggregation was apparently reversible. These results give a more comprehensive understanding of how to reliably control the structural and rheological properties of lamellar liquid crystals, and emphasise the importance of the size and surface chemistry of any inclusions, for applications in cosmetics, drug delivery, and microfluidics.

1 Introduction

Ternary phases composed of oil, water and surfactant are widely known to form different structures, ranging from isotropic solutions of micelles to ordered liquid crystal mesophases.[1] By careful selection of solvents and surfactants, and their ratio, it is possible to reliably tune a system to form these specific structures.[2] A typical ternary phase diagram is shown in Figure 1a, wherein the different coloured areas represent different monophasic regions, *i.e.* L_1 represents micelles, L_2 inverse micelles, L_3 a bicontinuous sponge phase, and L_α a lamellar bilayer system. Each of these specific phases has existing or potential uses in different industries, such as cubic, hexagonal, or lamellar systems being investigated for implementation in drug delivery,[3,4] as templates for mesoporous silica,[5,6] or as hosting media for protein crystallisation.[7]

Lamellar systems, comprising alternating hydrophobic (typically oleophilic, 'oil-loving') regions and hydrophilic ('water-loving') regions separated by ordered surfaces of surfactant, are a form of liquid crystal mesophase that are widely researched. This is largely due to their uses in food science and biotechnology, arising from their similarity with cellular structures,[3,8,9] or in microfluidics and nanotechnology as templating agents or thermal sensors[10,11]. Derived from their relatively simple structure, as portrayed in Figure 1b, is a known relationship between the interlamellar spacing, d (*i.e.* the repeat distance of the system on the axis perpendicular to the layers), the constant bilayer thickness, δ, and bilayer volume fraction, Φ:[12]

$$d = \frac{\delta}{\Phi} \quad (1)$$

To investigate the use of liquid crystal mesophases as biological models or in microfluidics, the effect of any added particles on the properties of the mesophase must be understood. In turn, this will guide understanding on the cytotoxicity of nanoparticles, endocytosis, lubricants, and complex fluids. It has been reported

[a] *School of Chemistry, Monash University, Clayton 3800, Australia. E-mail: joshua.marlow1@monash.edu*
[b] *Australian Centre for Neutron Scattering, Australian Nuclear Science and Technology Organisation, Lucas Heights, NSW 2234, Australia*

† Electronic Supplementary Information (ESI) available: Table of SANS results and bilayer thickness analysis. See DOI: 10.1039/b000000x/

that hydrophobic silica nanoparticles, for instance, can form gel structures when added to lipid monolayers.[13] In nematic liquid crystal droplets, polystyrene nanoparticles have been seen to aggregate into specific structures that are dependent on the properties of the liquid crystal.[14] For phospholipid lamellar phases, however, this causal relationship appears to be reversed, and the structures formed by hydrophobic silica nanoparticles present at domain boundaries have been found to promote phase transitions due to their curvature.[15] A similar effect was observed for hydrophilic nanoparticles in a lipid-like monoolein system; low concentrations of nanoparticles favoured the formation of a bicontinuous cubic gyroid phase.[16] Conversely, high nanoparticle concentration suppressed this phase in favour of a lamellar system.[16] Together, these results imply that as much as the mesophase may affect the distribution and location of any included or dispersed nanoparticles, the particles within may influence the mesophase to an even greater extent. The ability of included particles to influence mesophase architecture has been seen in both lamellar systems, where size has been shown to be an important factor,[17] and hexagonal systems.[18] This adds complexity, but also provides new opportunities for design and tuning of nanostructured complex media.

This study aims to provide a clearer understanding of how varying the composition (of oil, water, surfactant(s), and of added nanoparticles of differing size and surface chemistry) can alter the properties of a lamellar liquid crystal system. A lamellar system was used as these materials have a relatively simple geometry, allowing this work to later extend to other mesophases. The effects that these compositional parameters have on the structural and rheological properties of the resultant mesophases is important for the use of these systems as solvents, lubricants, or as biological models. In this context, 'structural' properties are defined as the mesophase identity and the characteristic dimensions of this phase, while 'rheological' properties refers to the viscoelasticity of the phase and the dynamics of any contained nanoparticles. This work also hopes to understand where nanoparticles are located within these systems, and how this arises from their interactions (or lack thereof) with the mesostructure.

A ternary phase of water, *p*-xylene and Triton X-100 was investigated as it features a relatively large lamellar region within its phase diagram (depicted in Figure 1a, as found from previous work[2]) that allows for easy modification of each component without changing the phase identity. The specific compositions investigated are shown in Table 1. To examine the effect of particle size and surface chemistry, three types of silica particles were used: 10 nm hydrophobic (modified by octylsilane) particles, 10 nm hydrophilic particles and 20 nm hydrophilic particles. Silica nanoparticles were used due to their ubiquity, ease of fabrication and potential for targeted application, such as tailoring for bactericidal purposes, which together make them appealing for research within cellular systems.[19]

As typical liquid crystals and lipid systems have shown different responses to the presence of contained particles, the response of these systems when adding a co-surfactant to increase the system's 'lipid-like nature' was investigated. This would also be important for the use of these systems as biological models, as cel-

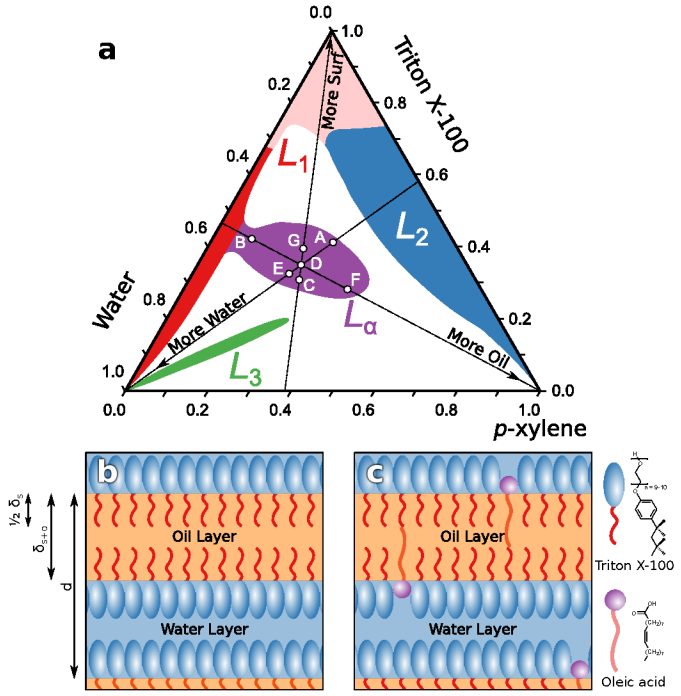

Fig. 1 (a) The ternary phase diagram for the system being studied with compositions A-G used in this study marked (see Table 1, adapted from previous work.[2]) L_1 corresponds to the micellar region, L_2 the inverse micellar region, L_3 the bicontinuous sponge region, and L_α the lamellar region. The lighter region in the Triton X-100 corner represents concentrated monophasic systems where no distinction was observed between L1 and L2, and the white areas represent multiphasic systems. (b) Schematic representation of a lamellar liquid crystal system comprising water, *p*-xylene and Triton X-100 (not to scale). The interlamellar spacing d, the thickness of an oil/surfactant bilayer δ_{s+o}, and half the surfactant bilayer thickness $\frac{1}{2}\delta_s$ are marked. (c) As (b) but with a fraction of the surfactant molecules replaced with oleic acid.

Table 1 Phase compositions for liquid crystal samples in the water/*para*-xylene/Triton X-100 system: composition name (Composition), mass fractions of water (m(Water)), *para*-xylene (m(*p*-Xylene), and Triton X-100 (m(Triton X-100). Further conditions are detailed in Table 2.

Composition	m(Water)	m(*p*-Xylene)	m(Triton X-100)
A	0.30	0.29	0.41
B	0.48	0.10	0.42
C	0.43	0.27	0.30
D	0.40	0.25	0.35
E	0.45	0.23	0.32
F	0.32	0.40	0.28
G	0.37	0.23	0.40

lular liquid crystal structures are formed by phospholipids. Different mass fractions of Triton X-100 (0.00, 0.04, and 0.08) were substituted with oleic acid in some samples to analyse how this substitution of a lipid-like secondary surfactant affected the properties of the liquid crystal. Oleic acid was used as it is a common, biocompatible surfactant that is known to form stiff structures, and can modulate mesophase textures when used as a secondary surfactant.[20–22] It also has a large hydrophobic moiety and a small hydrophilic head-group, making it a much more lipid-like surfactant than Triton X-100, which has the opposite properties in that respect. This distinction is highlighted in Figure 1b. By mixing the two surfactants in different ratios, we aimed to probe how surfactant structure can be utilised to tailor systems for specific properties. In turn, this will aid in the formation and use of liquid crystal models for cellular systems, or in other systems. Different contrast conditions, detailed alongside the above measuring conditions in Table 2, were also used to highlight structural changes.

Structural analysis and phase identification was performed via small-angle neutron scattering (SANS), polarising light microscopy (PLM), and rheological tests. Oscillatory amplitude sweeps were performed to examine how the storage and loss moduli (*G'* and *G"*, respectively) change as a function of increasing shear strain, in turn providing information on both the elastic and viscous response of the systems. Rotational viscosity curves were also performed to show how the viscosity of the samples changed with shear.

2 Materials and Methods

2.1 Materials

Triton X-100 (>98%) and oleic acid (>98%) were obtained from ChemSupply; Decane (>99%), *para*-xylene (anhydrous, $\geq$ 99%) and D_2O (99.8 atom % D) were purchased from Sigma-Aldrich; reagents were used as received. Water was obtained from a Milli-Pore Direct-Q 5, with a minimal resistivity of 18.4 MΩ·cm. Fumed silica nanopowders (both hydrophilic and hydrophobic, the latter modified by octylsilane) of the size range 7–14 nm were obtained from PlasmaChem GmbH, as was an aqueous 50% suspension of 20 nm SiO_2 nanoparticles. The suspension was freeze-dried prior to loading, while the other particles were used as delivered. Compositions were formulated within the lamellar region of the Triton X-100, water, *p*-xylene ternary system found in previous work (as shown in Figure 1a) and are presented in Table 1, while the measuring conditions are detailed in Table 2.[2] Particle sizes were confirmed using atomic force microscopy (AFM).

2.2 Small-angle neutron scattering

SANS Measurements were performed on the Bilby beamline at ANSTO, Lucas Heights, Australia.[23] Samples were prepared in 2 mm path-length quartz Hellma cells using D_2O, H_2O, or a mixture of the two to contrast-match the silica particles. In cases where D_2O was used, the masses were adjusted to achieve a consistent molar ratio of constituents amongst the different contrast variations. Data were reduced from the raw counts on a two dimensional detector and plotted as radially averaged absolute intensity *versus* the scattering vector q, under the assumption of isotropic scattering. The value of q is defined:

$$q = \frac{4\pi}{\lambda}\sin\frac{\theta}{2} \quad (2)$$

where λ is the wavelength of the incident neutron beam and θ is the angle of scattering. The q range is therefore determined by the instrument setup and detector size. Neutrons of incident wavelength λ = 5–9 Å were used with a sample-detector distance of 4.8 m, giving a q-range of 0.01–0.3 $Å^{-1}$. Data were reduced by normalising the response of each detector pixel via comparison with the response of a detector to a flat scatterer.

Characteristic distances within the structure were calculated by locating peaks in the scattered intensity and utilising the relationship:

$$d = \frac{2\pi}{q} \quad (3)$$

where d is the distance (*e.g.* interlamellar spacing for a lamellar system).

2.3 Rheological measurements

Rheological measurements were performed with an Anton Paar MCR-302 rheometer (Austria) using a cone-and-plate geometry with cone diameter of 40 cm and angle of 0.3°. A Peltier plate and evaporation blocking system were used to ensure the samples were kept at a constant 25°C with minimal evaporation. Each sample was loaded onto the plate carefully, and the cone was lowered to just above the measuring position, whereafter excess sample was scraped away. The cone was then moved to the measuring position. Measurements were taken after one minute of pre-shearing to erase any shear history imparted by loading.

2.4 Polarising light microscopy

Polarising light microscopy (PLM) images were obtained using a CMOS camera (Flea3, Point Grey, Richmond, BC, Canada) connected to a Kozo XJP-300 polarising microscope. Images were taken between crossed polarising filters.

3 Results and Discussion

3.1 SANS

Small-angle neutron scattering (SANS) was used for structural analysis within this work, and typical spectra obtained are presented in Figure 2. The lamellar phase is characterised by the

Table 2 Additives and contrast conditions utilised within these experiments, and to which compositions (see Table 1) they were applied. Sample names are constructed from the compositional name from Table 1 in addition to any measuring conditions, e.g. "B + 2.5% HB, d-xylene".

Measuring Condition	Description	Systems Applied To
"+ 4% OA"	Mass fraction of 0.04 of oleic acid replaced same mass fraction of Triton X-100	B
"+ 8% OA"	Mass fraction of 0.08 of oleic acid replaced same mass fraction of Triton X-100	B
"+ 1% HB"	1% 10 nm Hydrophobic Silica	A-G
"+ 2.5% HB"	2.5% 10 nm Hydrophobic Silica	B
"+ 1% HP"	1% 10 nm Hydrophilic Silica	A-G
"+ 2.5% HP"	2.5% 10 nm Hydrophilic Silica	B
"+ 1% 20 nm HP"	1% 20 nm Hydrophilic Silica	A-G
"+ 2.5% 20 nm HP"	2.5% 20 nm Hydrophilic Silica	B
"Mix"	Aqueous solvent was a 0.37 : 0.63 mass ratio of H_2O to D_2O to contrast match the silica particles	B
"Water"	Aqueous solvent was H_2O	B
"d-Xylene"	Aqueous solvent was H_2O; deuterated *para*-xylene was used	B
"D_2O"	Aqueous solvent was D_2O; if unspecified, this condition was used	A-G

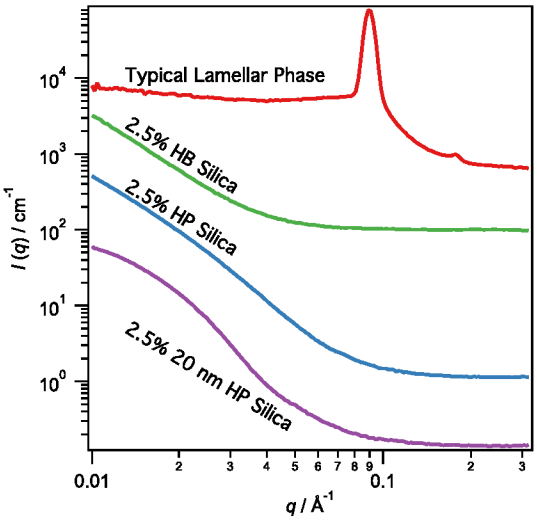

Fig. 2 A typical SANS spectrum for a lamellar phase compared to SANS spectra for the three particles used in this study. The data are vertically offset by an order of magnitude each for clarity.

presence of two relatively well-defined peaks at a q-ratio of 1:2, whereas the silica particles exhibit strong form factor scattering in the low q-region.

3.2 Contrast conditions for SANS

SANS was used to examine the phase behaviour of the systems outlined above, and a table detailing the peaks and lamellar spacings obtained from each of the samples can be found in the Supplementary Information†. The spectra for samples with different contrast environments are presented and compared in Figure 3.

It is firstly apparent, due to the spacing of the first- and second-order Bragg peaks in the majority of spectra, that composition B (see Table 1), regardless of doped silica particles, is a lamellar phase, with an interlamellar spacing of approximately 67 ± 1 nm. The intensity of these peaks (especially the second order peak) are lower for the *Mix* (utilising the silica-matched mixture of H_2O and D_2O) and *Water* (using just H_2O) contrast conditions (see Table 2 for more information), which is explained by the lower contrast in these conditions when compared to samples with a greater difference in neutron scattering length densities (such as the D_2O contrast setting). However, these contrast conditions also further highlight the effect of any contained silica particles on the low q region (*i.e.* below around 0.04 Å^{-1}) of the spectra – an effect also observed for the *d*-xylene contrast condition which does not feature the same decrease in intensity for the peaks that arise from the lamellar phase.

The low q region represents structures on larger scales than the interlamellar spacing, and scattering in this region is due to effects such as structure factor, scattering from extended surfaces, poorly defined interfaces, *etc.*[10] The model used, created by Nallet *et al.*, attributes this region to extended bilayer surfaces, however it has been known to fit this region poorly in some circumstances, potentially due to a departure from the idealised model.[10,24,25] In this case the lamellar systems present a low gradient, indicating such a divergence that likely arises from increased curvature or flexibility of the bilayers at larger length-scales.

Low, broad peaks potentially representing the form factor of the silica particles of 10 nm and 20 nm (*i.e.* at $q \approx 7$ Å^{-1} and $q \approx 0.3$ Å^{-1} respectively) are visible in the samples that contain them, however these peaks are not observed in the spectra of the particles alone (see Figure 2). This implies that the liquid crystal structure is causing some order on the size scale of the particles despite no apparent changes to the lamellar structure. These peaks may thus represent the surfactant coating and stabilising the particles, in turn bolstering the response to the form factor of the nanoparticles, which could in turn explain why these features are not observed within the samples containing no surfactant – this has been postulated previously with silica particles in liquid crystal and lipid structures.[15,17]

Additionally, the low q behaviour of both hydrophobic and hydrophilic 10 nm particles, as observed in Figure 2, likely due to the structure factor of the particles, is apparently retained for this composition. This effect is much less visible for the D_2O contrast condition, likely due to the silica providing weaker contrast than the deuterated water. The behaviour of the 20 nm particles' spectrum is not replicated, however, indicating that the liquid crystal disrupts some larger order that the 20 nm particles have when by themselves. This could indicate that these larger particles are favourably coated by surfactant, and as such are prohibited from forming larger networks.

It is worth noting that, as structural properties ascribed to the silica particles are visible in the silica-matched contrast condi-

tions, it may be inferred that the specific mixture of D_2O and H_2O did not perfectly contrast match the silica particles. An alternative explanation for this is that the contrast conditions succeeded in matching the silica particles, however if the surfactant formed a coating around the particles, these features would still be visible (as the surfactant shell would be a feature on the same size scale as the particle).

3.3 Effect of composition

Aside from composition F, all other systems examined were monophasic lamellar systems, as predicted by previous work.[2] Composition F, however, appeared to form an unidentified mono- or biphasic system, perhaps containing both the lamellar phase and some unidentified secondary phase. This additional phase may be an another lamellar system with a different spacing, or some other structure - however without isolation of this phase or observable higher order peaks, the identity cannot be unambiguously concluded from the current data. These spectra are shown in Figure 4, and further discussed later.

Regardless of whether any type of silica was added to the systems, increasing the mass fraction of solvents caused an increase in the interlamellar spacings, while increasing the mass fraction of the surfactant had the inverse effect. These results are expected, and the specific relationship is observed as per equation 1.[12] This linear relationship between the interlamellar spacing and the inverse volume fraction of surfactant is highlighted in Figure 5. This arises because a higher volume fraction of surfactant allows a larger surface area of membrane to form, thereby reducing the volume-to-surface ratio of the water and oil sections of the lamellar structure. Deviations from this behaviour are potentially due to effects such as holes within the sheets, more/less rigid sheets, increased tortuosity, *etc.*[12]

The bilayer thickness found as per Equation 1, when using $\delta = \delta_s$, *i.e.* considering the bilayer only where the surfactant is present, is 32 Å, which is below the fully extended molecular length of Triton X-100. and thus slightly less than half of the length one might expect for a bilayer of the molecule.[26] This discrepancy is likely due to the fact that the Triton X-100 is not fully extended, owing to flexibility of the PEG chain, and that the bilayer thickness is considered to only consist of the surfactant tails, not the heads.[26] This arises from the strong contrast length density step between the oligo(ethylene glycol) head-groups (which are heavily solvated by water), and the hydrocarbon tails. The adherence to Equation 1 despite which solvent fraction is changed also reveals that regardless of whether the oil or water layers are swelled, the bilayer thickness is unchanged, indicating that the surfactant tails form a close-packed layer which excludes the oil. The use of Equation 1 while considering a bilayer to consist of either solvent and the surfactant (e.g. $\delta = \delta_{s+o}$ for oil/surfactant bilayers) follow similarly linear trends.†

Changes in the low q region of the spectra were observed at different concentrations and notably these changes, unlike the quantitative relationship between surfactant mass fraction and lamellar spacing, were not consistent between all sample sets. As these systems all diverge from the expected model, there is little insight to be gained from this region.[10,24,25]

However, the fact that there is a change for different silica particles, in addition to the extra peaks observed for samples 'F + 1% HB', 'F + 1% HB 20 nm', 'C + 1% HB', and 'C + 1% HP', reveals that the presence of the silica particles *does* affect the structure of these systems, even if the interlamellar spacings remain unchanged. This extra peak is likely caused, in the case of composition F, by an alteration of the ternary phase diagram that pushes the composition, otherwise firmly within the lamellar region, across a phase boundary, due to the particles promoting a specific local curvature.[15,16] Alternatively, the ternary phase diagram may be different for heavy water - this could be confirmed with small-angle x-ray scattering (SAXS) measurements of these same systems.

The additional peaks observed for composition C phases seem to correspond to the sizes of the silica nanoparticles, but differ to the scattering of the particles alone, and therefore are likely due to interactions between the particles and the surfactant. The silica-promoted structures will be discussed further in the section that interrogates the effect of added silica particles.

3.4 Effect of lipid-like co-surfactant

Amplitude and viscosity sweep rheological measurements were undertaken to assess the effects of replacing fractions of the Triton X-100 surfactant, which contains a large, flexible hydrophilic group and a branched hydrophobic moiety, with oleic acid, which has a truncated hydrophilic group and relatively long carbon chain as its hydrophobic tail-group. These results are displayed alongside the corresponding PLM images and SANS spectra in Figure 6.

As seen in the amplitude sweeps, increasing the proportion of oleic acid causes several notable rheological changes to the samples. Both the storage and loss moduli (*G'* and *G"*) increase at all shear strain values, while the flow point (*i.e.* where the linear viscoelastic range ends) and crossover point (between the curves of *G'* and *G"*) both move to larger shear strain values. These effects indicate that the incorporation of oleic acid causes a rigidification of the overall structure, which requires a greater deformation to break when more oleic acid is present.[27] Further, the more pronounced peak in the *G"* curve for the samples with greater mass fractions of oleic acid indicates that this stiffening is accompanied (or caused) by a more consistent three-dimensional order within the system.[27,28].

As expected for lamellar systems, the liquid crystals examined herein are shear-thinning, as observed by a decreasing viscosity as applied shear rate is increased in Figure 6d-f,l. This can be explained by the shear force causing alignment of the lamellar bilayers in the direction of the applied stress.[29,30] Another possible effect of the shear is a region where the lamellar sheets form 'onions': concentric, layered pseudospherical shapes that can, at higher shear, return to the aligned bilayers.[29,30]

Similarly to the results from amplitude sweeps, the replacement of 4% w/w of the system with oleic acid causes an increase in the viscosity both before and after shear, however at 8% w/w of oleic acid, the return viscosity sweep unexpectedly achieves

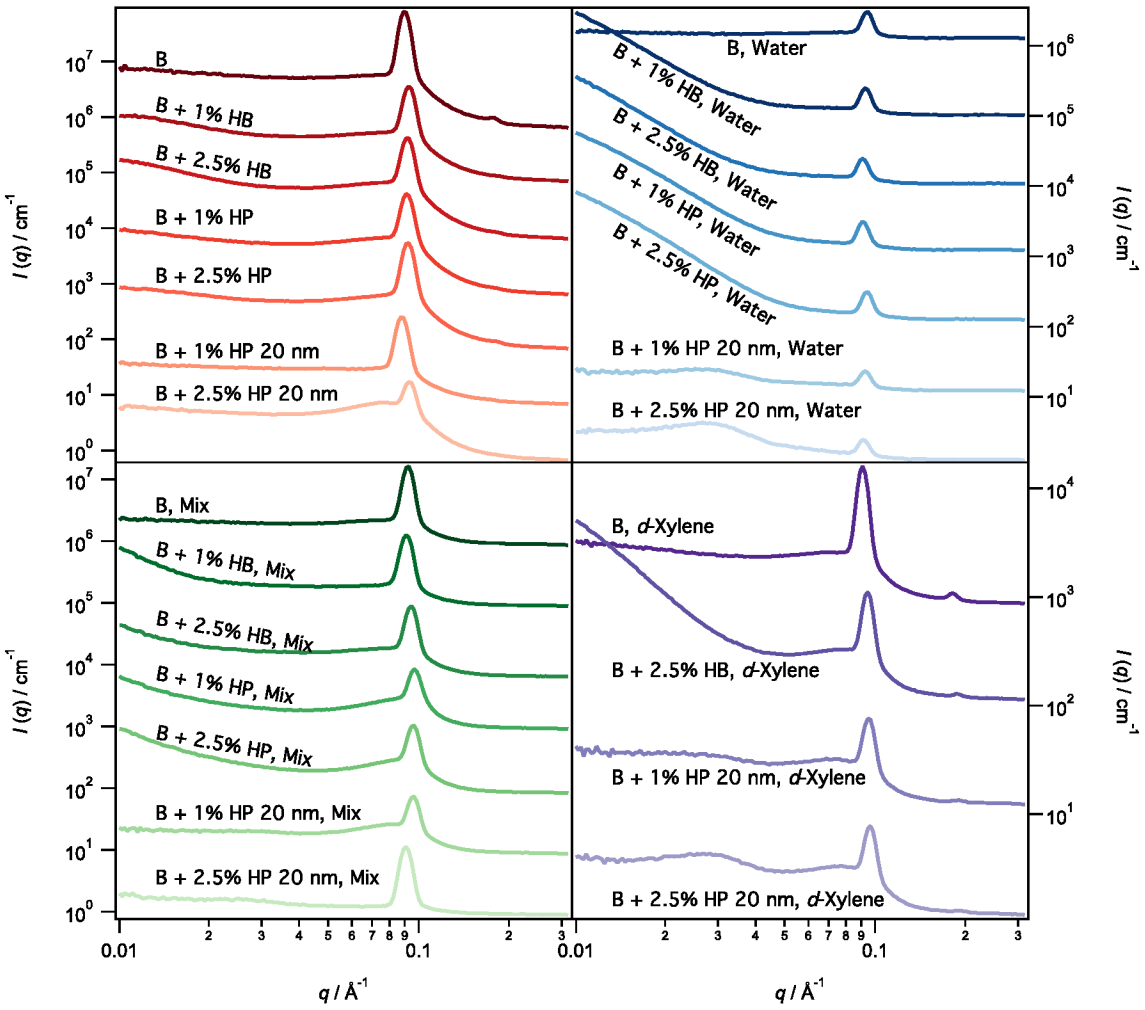

Fig. 3 Experimental SANS spectra for the examined water/*p*-xylene/Triton X-100 ternary phases with and without added silica nanoparticles in four different contrast conditions. From left to right, top to bottom: with D_2O, H_2O, in a silica-matched 0.37:0.63 mass ratio of H_2O:D_2O, and in H_2O with deuterated *p*-xylene. Individual spectra are each offset by a factor of magnitude for clarity. See Tables 1 and 2 for specific compositional information.

higher viscosity values than the forward sweep despite retaining the shear-thinning nature. This could be explained by the alignment of the system conferring a rigidity of some description, though the exact cause is unknown.

As observed within Figures 6k and l, these relationships of mass fraction of oleic acid with respect to the *G'* and *G"* values, and to the viscosity, are complicated when silica nanoparticles are added to the system – potentially due to the disruption of this three-dimensional network by the presence of these defects. These discrepancies will be discussed further in the section detailing effects of added silica particles.

Polarising light microscopy images of the samples were obtained and are presented in Figure 6g-i. Present for all three samples is a streaky, marble-like optical texture which is characteristic of lamellar phases, agreeing with the SANS spectra in Figure 6j.[31] The sample with no oleic acid, 'B', however, shows an interconnected set of 'oily streaks' which have been attributed to bundled 'disclinations', areas of abrupt orientation changes.[32] This may in turn imply that the introduction of oleic acid imparts some form of order that reduces this effect, however further study of these specific samples would be required to confirm this.

The SANS spectra of these systems, presented in Figure 6j, reveal that an increased loading of oleic acid increases the lamellar spacing (as evidenced by the movement of the first-order Bragg peak to lower *q* values) as well as potentially reducing the regularity of the lamellar sheets (as evidenced by the relative weakening of the second-order Bragg peak). This increase in bilayer spacing may be explained by the larger hydrophobic portion of the oleic acid molecule, or simply the two different surfactant molecules not packing well due to their similar sizes but relatively distinct shapes (for instance the unsaturation in the oleic tail).

While the rheological and PLM results imply that the oleic acid imparts a long-range order to the sample, the weakening of the peaks in the SANS results implies a loss of local order. This can possibly be described by the two forms of disorder: the first kind, in which lamellar sheets may thermally oscillate, causing a loss of long range order, and the second kind, where heterogeneities cause a loss of long range order.[33,34] By adding oleic acid, the bilayers become more rigid, reducing disorder of the first kind - however, as they only represent a fraction of the overall surfac-

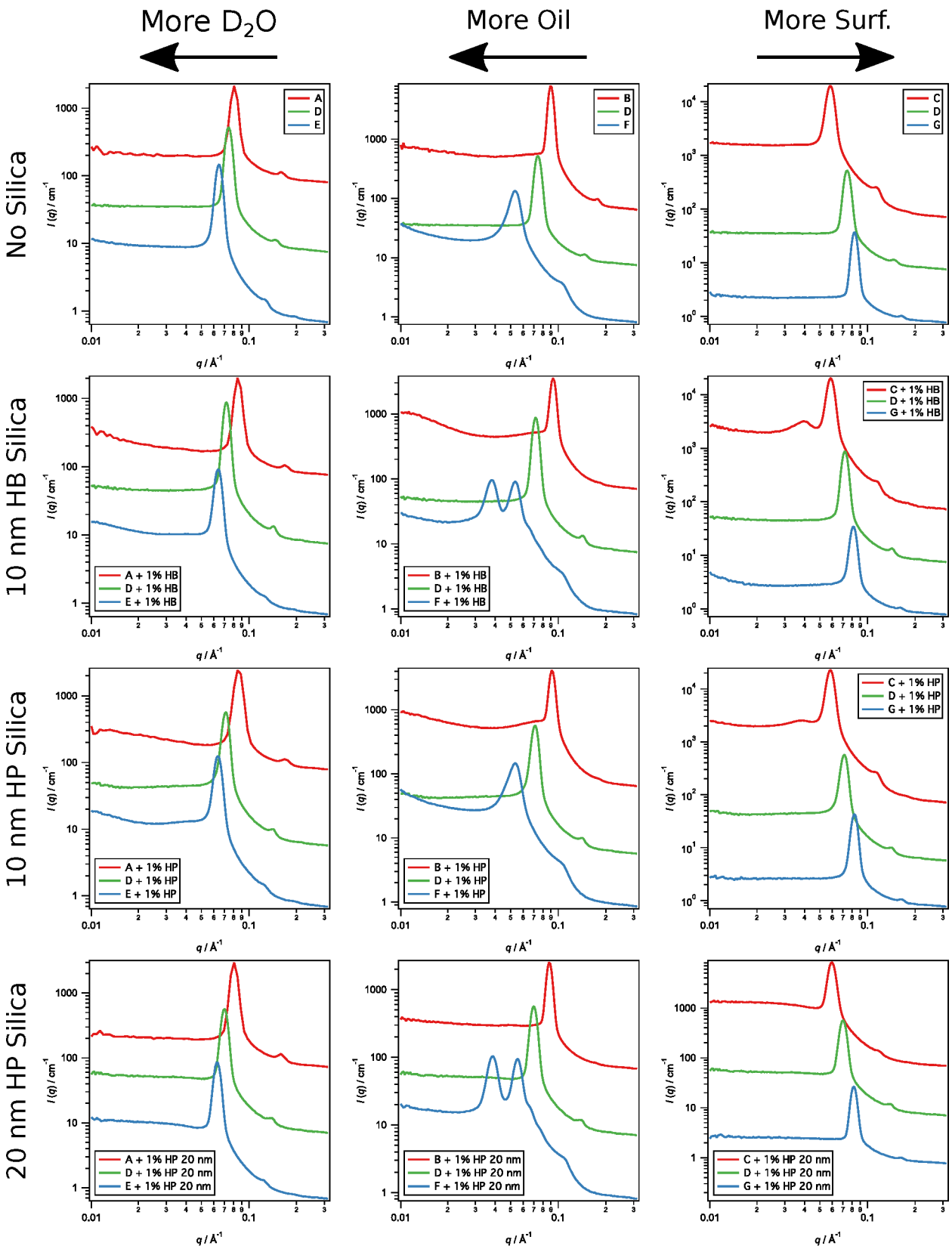

Fig. 4 Experimental SANS spectra for the examined water/*p*-xylene/Triton X-100 ternary phases with and without added silica particles. Spectra are each vertically offset by an order of magnitude for clarity. The keys refer to the samples' compositions and measuring conditions, as detailed in Tables 1 and 2.

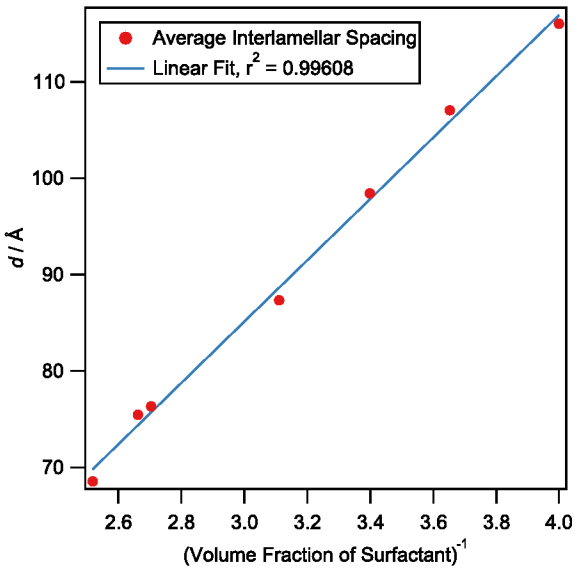

Fig. 5 The average (from samples with all varieties of silica particles) interlamellar spacing of liquid crystal samples A–I, taken from the SANS spectra, plotted as a function of the inverse volume fraction of the surfactant, Triton X-100. The least-squares fit is shown, corresponding to a constant bilayer thickness of 32 Å.

tant, their presence represents defects which cause disorder of the second kind.

3.5 Effect of added silica particles

The structural and rheological consequences of added hydrophobic and hydrophilic silica nanoparticles were investigated via SANS, PLM and rheological measurements, the results of which are presented in Figures 4 and 7.

Comparing the amplitude sweep measurement of sample B in Figure 6a to its equivalents with the silica nanoparticles in Figures 7a-c reveals that all forms of silica nanoparticles tested cause an increase in both the storage and loss moduli of the sample, suggesting a stiffer structure. However, in all cases the extent of the linear viscoelastic region is reduced, indicating that a lower shear strain is required to cause the material to flow.

The 10 nm hydrophobic and hydrophilic silica particles appear to form a three-dimensional network within the sample, as evidenced by the peak in *G"* – however this same structure is not observed for the 20 nm hydrophilic silica.[27,35] This interconnected structure is likely responsible for the differing low *q* behaviour in the SANS spectra for the 10 nm particles observed in Figures 3 and 7j, however the structure appears to be much more easily deformable for the hydrophobic silica, as evidenced by its earlier flow point (end of the linear viscoelastic region), crossover point and *G"* local maximum.

Notably, the presence of the 10 nm particles appears to cause a greater ability to recover the structure of the sample, as evidenced by the smaller gap between the forward and backward amplitude sweeps and viscosity curves in Figures 7a–f, compared to the sample without silica, in Figures 6a and d. This effect, much like the apparent loss of a three-dimensional network, was the opposite with the 20 nm particles, which displayed a much lower recovery of the initial viscosity and storage/loss moduli. However, the presence of the 20 nm particles also causes a greater stiffness of the systems despite this. Overall, this indicates that the size of these nanoparticles is incredibly important to how they effect the rheological properties and structure of the system they are in even though the local environment, as per the SANS spectra in Figure 7j, appear largely the same. These effects are likely due to the larger nanoparticles being more likely to be coated in lamellar bilayers (because they are larger, less energy is required to 'bend' the structure around the particles), therefore any aggregation is reversible.[17] Therefore, the application of a small amount of shear likely separates these particles, explaining the small linear-viscoelastic region, and thus a longer relaxation time is likely required to recover the original structure, as evidenced by the low recovery on the same timescale of the other systems. Conversely, as the smaller nanoparticles are unlikely to be coated by surfactant, they form aggregates which require more energy to break apart, and will fragment into individual nanoparticles, therefore the recovery time is shorter, and on the same timescale the recovery of *G'* and *G"* is greater.

Much like the PLM images for the samples with oleic acid, the PLM images of the samples with silica, presented in Figures 7g-i all present with the same marbling texture, indicative of lamellar phases.[31] As with the samples containing oleic acid, the network of disclinations is not observed, potentially corroborating the theory that this structure is disfavoured with the greater long range order imparted by oleic acid or silica nanoparticles. Notably, sample 'B + 1% HB' had a low intensity of birefringence, implying the short range order was reduced. This seems to support the evidence in the amplitude sweep in 7a that the presence of the hydrophobic particles imparts some form of long range order (hence the larger rise in the *G" graph*) while disrupting the lamellar structure on a short range (hence the much shorter linear viscoelastic region).

As per the SANS spectra presented in Figures 3 and 7j, the addition of silica nanoparticles does not appear to alter the interlamellar distances of the liquid crystals, indicating that any structural effects they have are likely on a larger scale (*i.e.* the crystal domains and/or nanoparticle aggregates). The SANS spectra also appear to corroborate the aforementioned observation that this new order imparted by the silica nanoparticles in turn disrupts the order of the lamellar phase, as, in addition to the shorter linear viscoelastic regions observed in Figures 7a and c, and the aforementioned weakened birefringence for sample 'B + 1% HB', the second-order Bragg peak is greatly reduced when particles are added. Specifically, the weakening of both Bragg peaks in addition to the apparent drift to lower *q* implies introduction of disorder of the second kind, the loss of long-distance order of the lamellar phase, due to a reduction in domain size.[33,34] This disorder is likely responsible for the discrepancy in the viscoelastic property of samples with oleic acid when silica nanoparticles are added, as mentioned above in the section on the effect of oleic acid and portrayed in Figures 6k and l.

This weakening of the lamellar structure is the opposite effect to what has been observed for particles small enough to be included within the lamellar structure.[36] This indicates that even

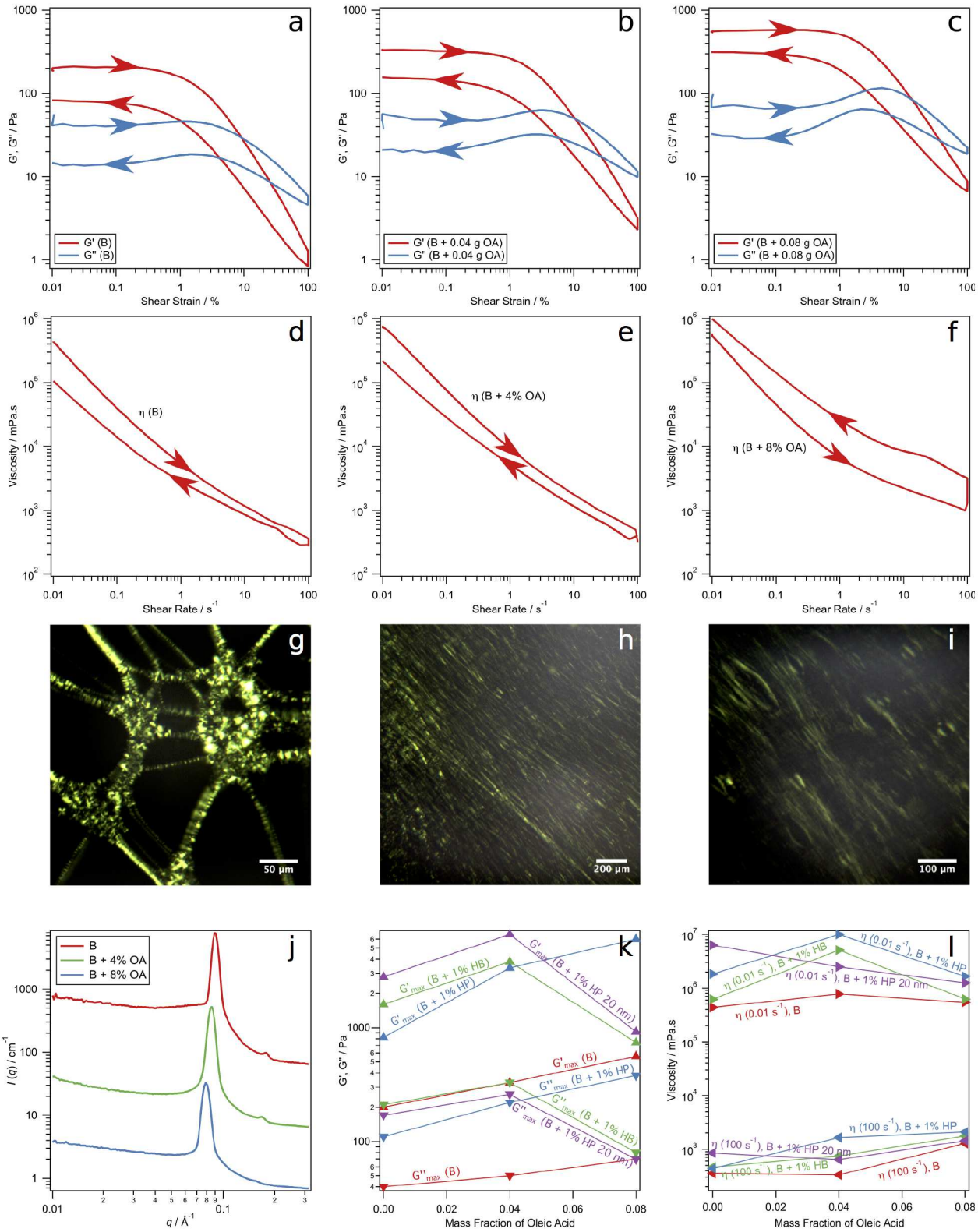

Fig. 6 The effect of replacing a proportion of Triton X-100 with oleic acid (OA) in sample B. (a-c) Dependence of the storage (*G'*) and loss (*G"*) moduli of the liquid crystal system as a function of shear strain, performed as an amplitude sweep moving in the direction of the arrowheads. (d-e) Viscosity curves of the samples, performed in the direction of the arrowhead. Both amplitude and viscosity sweeps were conducted with one minute at the initial shear strain/rate, and another minute kept at maximum shear before return sweeps were performed. (g-i) PLM images of the respective systems, taken between crossed polarisers. (j) SANS spectra of the liquid crystals, each offset by 10x. (k) Dependence of *G'* and *G"* in the linear viscoelastic region (LVR) on the mass fraction of oleic acid. (l) Dependence of the viscosity of the sample at 0.01 s^{-1} and at 100 s^{-1} on the mass fraction of oleic acid. The lines in (k) and (l) are to guide the eye.

at 10 nm these particles are large enough that they will be excluded from the thinner lamellar membranes and thus aggregate at, or whilst aggregated move to, domain boundaries – this behavior has been observed for other systems where the particle size is much larger than a liquid crystal's characteristic spacing.[17,36,37] This behavior is potentially due to the fact that the presence of these larger particles within layers thinner than their diameter would require these lamellar structures to bend around the particles (which should also be visible as an additional or spread out SANS feature); this would likely be energetically unfavourable. This further emphasises the importance of size when dealing with inclusions and defects.

4 Conclusions

The structural and rheological consequences of altering the composition of a lyotropic lamellar liquid crystal phase have been examined. Specifically, the effects of changing the mass fraction of each component, mixing in a secondary surfactant with markedly different molecular geometry to increase the lipid-like nature of the system, and adding silica nanoparticles were explored. Phase identities were characterised using small-angle neutron scattering and polarising light microscopy, the former of which also provided insight into the interlamellar spacing and the membrane order. Amplitude and viscosity sweeps were performed with a benchtop rheometer to assess how these variables affected the long-range order of these systems as well as their flow properties.

It was found that, while remaining within the lamellar region of the ternary phase diagram, the interlamellar spacing varied inversely with volume fraction of surfactant, representing a constant bilayer thickness, δ_s, of 32 Å. This thickness is found to increase when a secondary surfactant, oleic acid, is added, due to either the larger hydrophobic region of the oleic acid molecule or less efficient packing in the bilayer. Addition of the oleic acid was found to also cause an apparent disruption of the repeat lamellar order due to representing a substitutional defect, while rigidifying the overall structure due to its lipid-like nature. These effects are shown schematically in Figure 8b. Added nanoparticles appeared to strengthen this new network, however there appeared to be a disruption between the effects of both when oleic acid was at a mass fraction of 0.08, especially for the 20 nm particles and the hydrophobic particles.

Without the oleic acid, 10 nm hydrophilic and hydrophobic silica nanoparticles, and 20 nm hydrophobic particles still appeared to form longer-range structures at the cost of repeat lamellar layering. These structures are most likely particle aggregates at the domain boundaries, which in turn cause a reduction in the liquid crystal domain sizes. The 20 nm nanoparticles are likely coated with surfactant, and are thereby reversibly aggregated, unlike the 10 nm nanoparticles whose aggregation appears to be permanent. For the 10 nm particles, the hydrophobic silica appeared to form stronger aggregates than the hydrophilic silica, though otherwise their properties were quite similar. Graphical representations of these theorised structures are given in Figures 8c and d. In certain systems, the presence of the silica particles appears to push the liquid crystal to become a biphasic system, and future analysis of these systems with small-angle x-ray scattering and polarising light microscopy may help to further understand what additional phase is present and why.

These results show that lamellar phases in the water/Triton X-100/*p*-xylene system feature closely packed layers of surfactant which exclude solvent, allowing ideal swelling and precise spatial control of the systems via compositional changes. By replacing small fractions (0.04-0.08% w/w) of the surfactant with the lipid-like oleic acid, the surfactant layers appear to rigidify, increasing longer-range order and making the system more viscoelastic. Doping of the oleic acid also causes the sheets to widen, attributed to less efficient packing of the molecules, and possibly causes a coincident loss of long-range order due to its disruption of the homogeneity of the surfactant bilayers. The introduction of different types of silica nanoparticles show that both the size and surface chemistry of any inclusions will drastically alter the effects the contained particles will have on the liquid crystal structure. In all cases, however, a long-range order was imparted, attributed to aggregation at domain boundaries. These aggregates also appeared to cause smaller domain sizes, and in some instances a phase transition. Larger particles are theorised to be coated in a layer of surfactant, causing the specific rheological properties they imparted, though further measurements, including recovery experiments, would be required to confirm this.

The discovery that particles larger than the lamellar bilayers are present or aggregate at the boundaries is consistent with previous work in the area, as is the notion that this may induce phase transitions.[15–17] However, to the authors' knowledge, this is the first instance where such aggregation is considered with respect to the long-range order, the domain sizes, and the rheological properties of these systems. Specifically, that this aggregation appears to cause a reduction in the liquid crystal domain size and thus an increase in disorder of the second kind. When the liquid crystals are made more lipid-like with the addition of oleic acid, to better resemble biological systems, the silica particles still stiffen the system, likely due to the formation of these aggregates. However, unlike in systems without particles, addition of more oleic acid doesn't always cause a stronger network, indicating that particles excluded from the mesophases cause a disruption of the order imparted by the stiffer membranes caused by the presence of more lipid-like molecules.

These findings facilitate fine control of lamellar liquid crystal systems via alteration of the composition and addition of nanoparticles or a co-surfactant. A more complete understanding of the microstructure of these systems was gained via analysis and comparison of structural and rheological data. The results also emphasise the need to carefully select what kind of particles are used within a given system, for use of the mesophase as a solvent or model, as subtle differences in size or chemistry can impart widely different properties. More broadly, the results inform the fate and location of nanomaterials in bilayer systems, relevant to cytotoxicity, endocytosis and nanomedicine.

5 Acknowledgements

We acknowledge the support of the Australian Centre for Neutron Scattering, Australian Nuclear Science and Technology Organisation, in providing the neutron research facilities used in this work

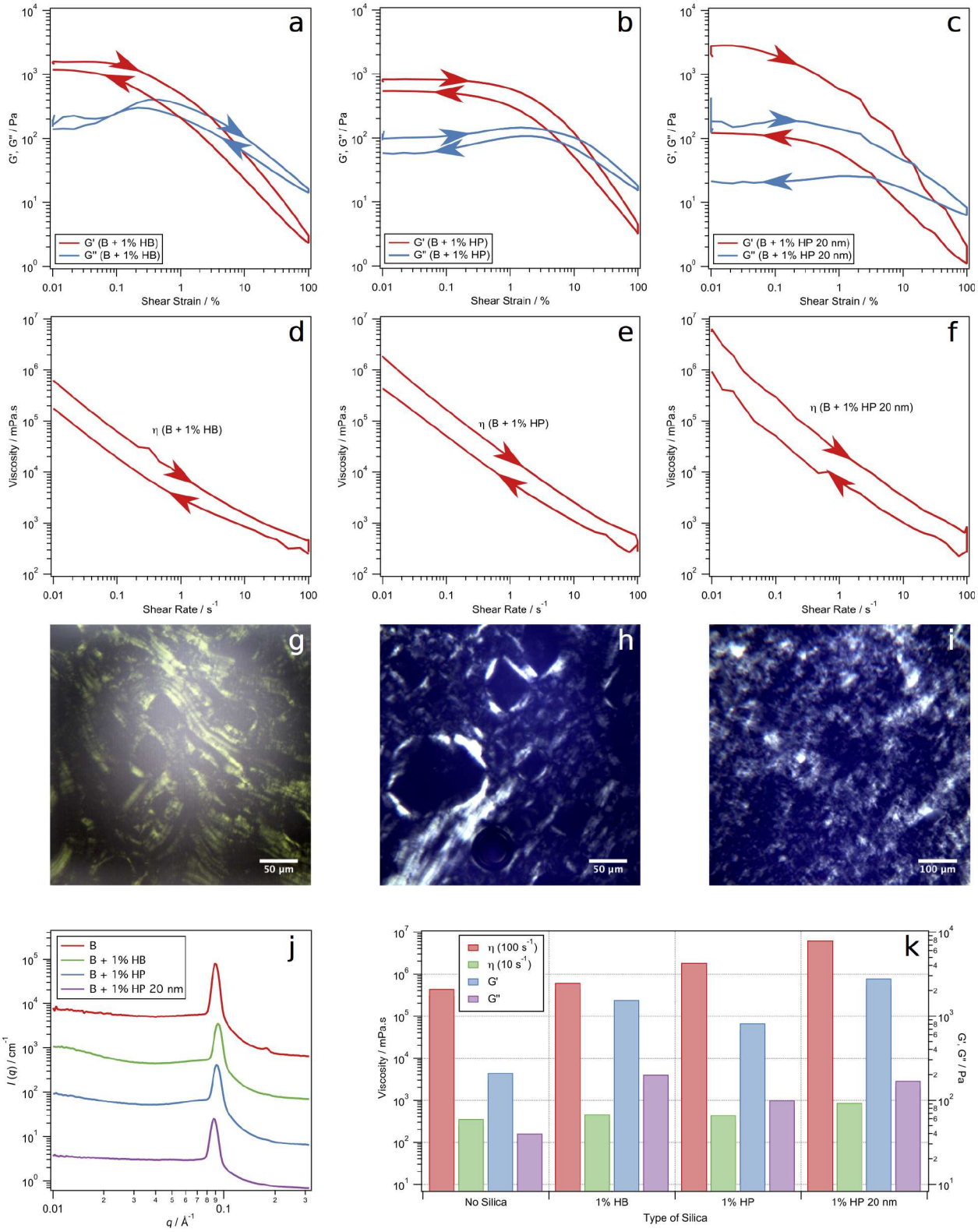

Fig. 7 The effect of adding silica nanoparticles to a ternary system of water/*p*-xylene/Triton X-100. (a-c) Dependence of the storage (*G'*) and loss (*G"*) moduli of the liquid crystal system as a function of shear strain, performed as an amplitude sweep in the direction of the arrowheads. (d-f) Viscosity curves of the samples, performed in the direction of the arrowhead. Both amplitude and viscosity sweeps were conducted with one minute at the initial shear strain/rate, and another minute kept at maximum shear before return sweeps were performed. (g-i) PLM images of the respective systems, taken between crossed polarisers. (j) SANS spectra of the liquid crystals, each offset by 10x. (k) Comparison of the viscosity at 100 s^{-1} and 0.01 s^{-1} (i.e. high and low shear respectively) and the storage and loss moduli for systems with each kind of silica particle.

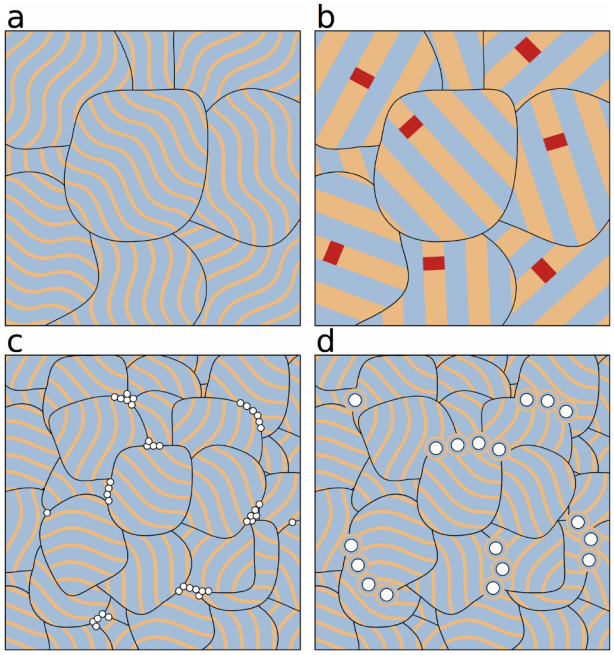

Fig. 8 Theorised microstructure of the examined lamellar liquid crystal (LC) systems, where orange represents the surfactant/oil bilayers, blue represents water, and black lines represent domain boundaries. (a) Domains of an LC with flexible bilayers. (b) An LC with added oleic acid (red). The bilayers are more rigid which increases ordering, but also contain oleic acid 'defects' which reduce ordering. The interlamellar spacing is also increased due to thicker bilayers. (c) An LC with added 10 nm silica particles. The silica nanoparticles form larger structures at the domain boundaries, and cause a reduction in the size of domains without affecting the bilayer structure. (d) An LC with added 20 nm silica particles. As with 10 nm particles, the silica forms larger structures, which cause a reduction in LC domain size, though these silica structures are likely easily-deformable due to a surfactant coating around the larger particles.

and the Australian Institute of Nuclear Science and Engineering for travel support for T.M.M. This work was supported in part by a Future Fellowship to R.F.T. from the Australian Research Council: FT160100191.

References

1 D. J. Mitchell, G. J. Tiddy, L. Waring, T. Bostock and M. P. McDonald, *J. Chem. Soc., Faraday Trans. 1*, 1983, **79**, 975–1000.

2 R. F. Tabor, M. I. Zaveer, R. R. Dagastine, I. Grillo and C. J. Garvey, *Langmuir*, 2013, **29**, 3575–3582.

3 M. Lapteva and Y. N. Kalia, *Skin Permeation and Disposition of Therapeutic and Cosmeceutical Compounds*, Springer, Tokyo, 2017, pp. 153–161.

4 Y. Chen, P. Ma and S. Gui, *BioMed Research International*, 2014, **2014**, 1–12.

5 J. W. Long, B. Dunn, D. R. Rolison and H. S. White, *Chemical Reviews*, 2004, **104**, 4463–4492.

6 D. A. Higgins, S. C. Park, K.-H. Tran-Ba and T. Ito, *Annual Review of Analytical Chemistry*, 2015, **8**, 193–216.

7 A. Zabara, T. G. Meikle, J. Newman, T. S. Peat, C. E. Conn and C. J. Drummond, 2017, **9**, 754–763.

8 J. Korlach, P. Schwille, W. W. Webb and G. W. Feigenson, *Proceedings of the National Academy of Sciences*, 1999, **96**, 8461–8466.

9 M. J. Pottage, T. L. Greaves, C. J. Garvey, S. T. Mudie and R. F. Tabor, *Soft Matter*, 2015, **11**, 261–268.

10 M. J. Pottage, T. Kusuma, I. Grillo, C. J. Garvey, A. D. Stickland and R. F. Tabor, *Soft Matter*, 2014, **10**, 4902–4912.

11 Z. Cong, B. Lin, W. Li, J. Niu and F. Yan, *Langmuir*, 2017, **33**, 7147–7151.

12 R. Strey, R. Schomäcker, D. Roux, F. Nallet and U. Olsson, *Journal of the Chemical Society, Faraday Transactions*, 1990, **86**, 2253–2261.

13 D. Orsi, T. Rimoldi, E. Guzmán, L. Liggieri, F. Ravera, B. Ruta and L. Cristofolini, *Langmuir*, 2016, **32**, 4868–4876.

14 M. Rahimi, T. F. Roberts, J. C. Armas-Pérez, X. Wang, E. Bukusoglu, N. L. Abbott and J. J. de Pablo, *Proceedings of the National Academy of Sciences*, 2015, **112**, 5297–5302.

15 J. M. Bulpett, T. Snow, B. Quignon, C. M. Beddoes, T.-Y. D. Tang, S. Mann, O. Shebanova, C. L. Pizzey, N. J. Terrill, S. A. Davis and W. H. Briscoe, *Soft Matter*, 2015, **11**, 8789–8800.

16 C. M. Beddoes, J. Berge, J. E. Bartenstein, K. Lange, A. J. Smith, R. K. Heenan and W. H. Briscoe, *Soft Matter*, 2016, **12**, 6049–6057.

17 E. Venugopal, V. K. Aswal and G. Kumaraswamy, *Langmuir*, 2013, **29**, 9643–9650.

18 S. Kulkarni and P. Thareja, *Rheologica Acta*, 2016, **55**, 23–36.

19 A. Tripathy, P. Sen, B. Su and W. H. Briscoe, *Advances in Colloid and Interface Science*, 2017, **248**, 85–104.

20 C. V. Nikiforidis, E. P. Gilbert and E. Scholten, *RSC Adv.*, 2015, **5**, 47466–47475.

21 C. Guo, J. Wang, F. Cao, R. J. Lee and G. Zhai, *Drug Discovery Today*, 2010, **15**, 1032–1040.

22 M. Nakano, T. Teshigawara, A. Sugita, W. Leesajakul, A. Taniguchi, T. Kamo, H. Matsuoka and T. Handa, *Langmuir*, 2002, **18**, 9283–9288.

23 A. Sokolova, J. Christoforidis, A. Eltobaji, J. Barnes, F. Darmann, A. E. Whitten and L. de Campo, *Neutron News*, 2016, **27**, 9–13.

24 F. Nallet, R. Laversanne and D. Roux, *Journal de Physique II*, 1993, **3**, 487–502.

25 F. Castro-Roman, L. Porcar, G. Porte and C. Ligoure, *The European Physical Journal E*, 2005, **18**, 259–272.

26 R. F. Tabor, J. Eastoe, P. J. Dowding, I. Grillo, R. K. Heenan and M. Hollamby, *Langmuir*, 2008, **24**, 12793–12797.

27 T. G. Mezger, *The Rheology Handbook, Third Edition*, Vincentz, Hannover, 3rd edn, 2011.

28 T. G. Mezger, *Applied Rheology*, 2015.

29 O. Diat, D. Roux and F. Nallet, *Journal de Physique II*, 1993, **3**, 1427–1452.

30 A. R. Sampaio, N. M. Kimura, B. L. Pelegrini, M. M. d. S. Lima and M. B. L. Santos, *Phase Transitions*, 2017, **0**, 1–10.

31 S. T. Hyde, *Handbook of Applied Surface and Colloid Chemistry*, J. Wiley and Sons, 2001, pp. 299–332.

32 K. Hiltrop, *Liquid Crystals*, Springer, 1994, pp. 143–171.

33 S. Förster, A. Timmann, M. Konrad, C. Schellbach, A. Meyer, S. S. Funari, P. Mulvaney and R. Knott, *The Journal of Physical Chemistry B*, 2005, **109**, 1347–1360.

34 G. Pabst, N. Kučerka, M.-P. Nieh and J. Katsaras, *Liposomes, Lipid Bilayers and Model Membranes: From Basic Research to Application*, CRC Press, 2014.

35 R. Mezzenga, C. Meyer, C. Servais, A. I. Romoscanu, L. Sagalowicz and R. C. Hayward, *Langmuir*, 2005, **21**, 3322–3333.

36 Y. Suganuma, M. Imai and K. Nakaya, *Applied Crystallography*, 2007, **40**, s303–s306.

37 S. Kulkarni, A. Verma, N. S. Mishra and P. Thareja, *Journal of Rheology*, 2017, **61**, 311–325.

TOC Entry

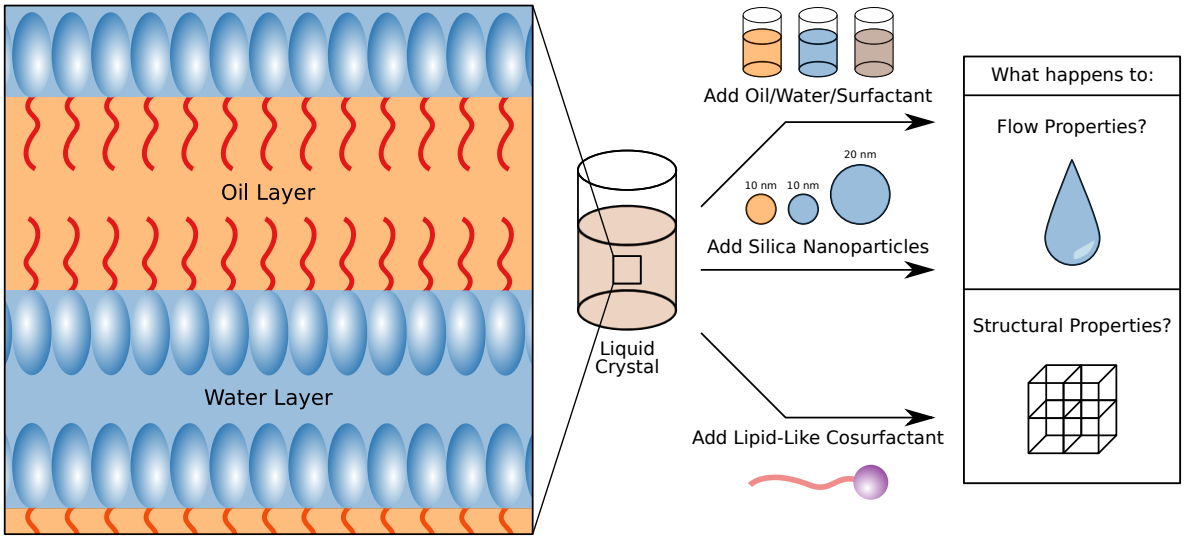

By adding silica nanoparticles to lamellar liquid crystals, their flow and structure can be changed dramatically, indicating new ways to understand particle–membrane interactions.